http://dx.doi.org/10.5012/bkcs.2013.34.11.3211

Density Functional Theory Study on D-π-A-type Organic Dyes Containing Different Electron-Donors for Dye-Sensitized Solar Cells

Jing Song* **and Jie Xu†**

*College of Accounting, Wuhan Textile University, 430020, Wuhan, China. *E-mail: jesute@hotmail.com*
†College of Materials Science & Engineering, State Key Laboratory of New Textile Materials & Advanced Processing Technology, Wuhan Textile University, 430020, Wuhan, China
Received March 29, 2013, Accepted August 1, 2013

Density functional theory (DFT) and time-dependent DFT (TD-DFT) calculations have been employed to investigate the molecular structures and absorption spectra of three D-π-A-type organic dyes (C1-1, D5 and TH208) containing identical π-spacers and electron acceptors, but different aromatic amine electron-donating groups (tetrahydroquinoline, triphenylamine and phenothiazine). The coplanar geometries indicate that the strong conjugation is formed in the dyes. The electronic structures suggest that the intramolecular charge transfer from the donor to the acceptor occurs, and the electron-donating ability of tetrahydroquinoline is stronger than those of triphenylamine and phenothiazine. The computed orbital energy levels of these dyes confirm that the electrons could be injected from the excited dyes to the semiconductor conduction band and the oxidized dyes could be reduced effectively by electrolyte. The TD-DFT results show that the CAM-B3LYP/6-31+G(d, p) is suitable for calculating the absorption spectra. The first absorption band for these dyes is assigned to the HOMO → LUMO and HOMO-1 → LUMO transitions.

Key Words : Dye-sensitized solar cells, Density functional theory, D-π-A, Organic dyes, Absorption spectra

Introduction

Dye-sensitized solar cells (DSSCs) have attracted significant attention in recent years as they offer the possibility of low-cost conversion of photovoltaic energy.[1] The dye sensitizer carries out the light-harvesting function in DSSC and is therefore crucial in determining the overall cell efficiency. The most successful sensitizers employed in these cells are ruthenium polypyridyl complexes, achieving up to 11% conversion efficiencies under standard air mass (AM) 1.5 illumination.[2-4] However, the Ru complexes are nevertheless costly and hardly attained, which will restrict the large-scale application of DSSCs.[5] Metal-free organic dyes as sensitizers have also been under intensive investigation due to their high molar extinction coefficients, flexible structural modifications and low costs.[6,7]

In the DSSC process, the dye first absorbs solar light to form the excited state. The excited electron is injected into the conduction band (CB) of the semiconductor (*e.g.* TiO_2), and then transported toward the counter electrode through electron diffusion. The oxidized dye is reduced back to its neutral state by the redox couple with the positive charge being transported from the electrolyte to the counter electrode. Thus, the lowest unoccupied orbital (LUMO) of the sensitizer must be located above the semiconductor CB to provide the thermodynamic driving force for favorable interfacial electron injection; the highest occupied molecular orbital (HOMO) energy should have a lower energy than that of electrolyte to accept the electron from a redox electrolyte pair. The overall efficiency of DSSC strongly depends on the following factors: (i) light-harvesting efficiency of the dye for solar spectrum; (ii) electron injection probability from the excited state of the dye to the semiconductor (efficiency of the charge separation); (iii) electron transfer probability from the electrolyte to the oxidized dye.[8] These factors are closely related with the ground and excited electronic states of the dye. Thus, it is very imperative to investigate the electronic structures of the dye not only for understanding the mechanism of the charge separation and transfer, but also for designing and synthesizing more efficient dyes.

Donor-(π-bridged)-acceptor (D-π-A) dyes are considered to be one of the most promising types of organic sensitizers. The photo-excitation of a D-π-A dye can induce the intramolecular charge transfer (ICT) from the donor to the acceptor, accompanied by efficient electron transfer through the acceptor from the excited dye into the semiconductor CB. The charge transfer or separation between the donor and acceptor in the excited dye may facilitate the electron injection from the dye into the semiconductor CB. The donor plays an important role not only in tuning and modifying the absorption spectra, but also in controlling the molecular energy levels and the intramolecular charge separation. Many types of donor groups have been explored in sensitizers, such as carbazole, coumarin, triphenylamine (TPA), indoline, tetrahydroquinoline (THQ), bis-dimethylfluorenylamino and phenothiazine (PTZ). Recently, Sun *et al.*[9] reported three dyes (the phenothiazine dye (TH208), triphenylamine dye (D5) and tetrahydroquinoline dye (C1-1), as shown in Fig. 1) which consist of different aromatic amine electron-donating groups, yielding overall efficiency of 5.6%, 4.8% and 4.4%, respectively.

In this work, to understand how and why the chemical

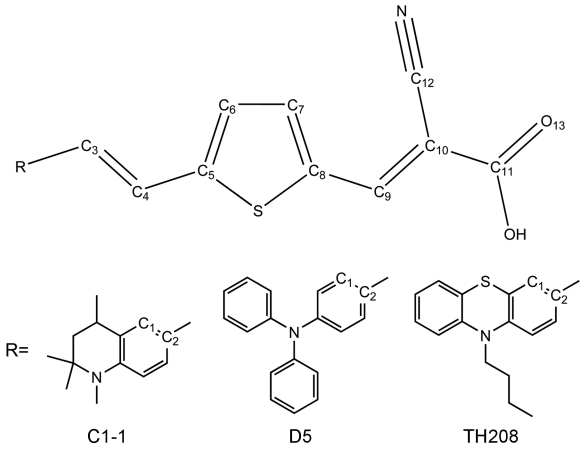

Figure 1. The structures of organic dyes C1-1, D5 and TH208.

modifications bearing the donor tune the electronic and spectroscopic properties of D-π-A dyes, density functional theory (DFT) and time-dependent DFT (TD-DFT) calculations were performed to study the geometries, electronic structures and absorption spectra of C1-1, D5 and TH208. DFT has emerged as a reliable standard tool for the theoretical treatment of the electronic structures and absorption spectra. TD-DFT can give reliable values for valence excitation energies with the standard exchange-correlation functionals. The computational cost of TD-DFT calculation is comparative to that of a Hartree-Fock based single excitation theory, such as, configuration interaction singles (CIS) or time-dependent Hartree-Fock (TD-HF) method and maintains a uniform accuracy for open-shell and closed-shell systems. DFT has been extensively used to study the structures and absorption spectra of sensitizers for DSSCs.[2,10-27]

Computational Details

All calculations were carried out with the Gaussian 09 package.[28] The ground-state geometries were fully optimized without any symmetry constrains at the DFT level of theory with Becke's[29] three parameters hybrid functional and Lee, Yang and Parr's correlational functional B3LYP[30] using 6-31G(d) basis set on all atoms. The natural bond orbital (NBO) characteristics were obtained by the second-order perturbation theory (SOPT) analysis.[31] The excitation energies and oscillator strengths for the lowest 30 singlet-singlet transitions based on the optimized ground-state geometry were calculated within the TD-DFT methodology using the 6-31G(d) basis set and the functionals B3LYP, CAM-B3LYP,[32] long-range corrected (LC) ωPBE,[33,34] ωB97XD,[35] MPW1B95[36] and PBE1PBE.[37] The absorption spectra are very sensitive to the basis set extension, and the simultaneous addition of extra polarization, diffuse and valence functions would lead to about 15 nm change of spectra. Thus, 6-31G(d), 6-31+G(d, p) and 6-311+G(2d, 2p) basis sets were then used to examine how the basis set affects the calculated excitation properties. The linear-response conductor polarizable continuum model (LR-CPCM)[38,39] was adopted here to include the bulk solvent effects (CH_2Cl_2). The UV-vis spectra were simulated using the SWizard program (Revision 4.6)[40] with the full width at half-maximum of 3000 cm^{-1}.

Results and Discussion

Ground-state Geometries. Figure 2 shows the optimized geometries of C1-1, D5 and TH208, which follow the same picture. Most of the corresponding parameters for D5 are in good agreement with the results calculated by Zhang *et al.*,[26] thus indicating the reasonability of the proposed results. All C–C lengths in the vinylene, thiophene and phenyl groups are between the distance of a single bonded C–C and a double bonded C=C, implying that there exists extensive delocalization throughout the molecules. The calculated distances between the C_2 atom and the C_{11} atom are 9.68, 10.24 and 10.24 Å for C1-1, D5 and TH208, respectively, indicating that the distance between the electron donor and semiconductor surface for C1-1 is shorter than those for D5 and TH208 and that the THQ group possibly have stronger electron-donating ability than the TPA and PTZ groups.

The cyanoacrylic acid group (acceptor) is found to be fully coplanar with the thiophene group (π-bridge), as represented by the C_7-C_8-C_9-C_{10} dihedral angles; while the donor group and the π-bridge are also arranged in an almost perfectly coplanar disposition. Thus, it can be concluded that the donor and acceptor moieties are fully conjugated through the π-bridge. The delocalization in the conjugate bridge is beneficial to the ICT and to the stability of the molecule. The

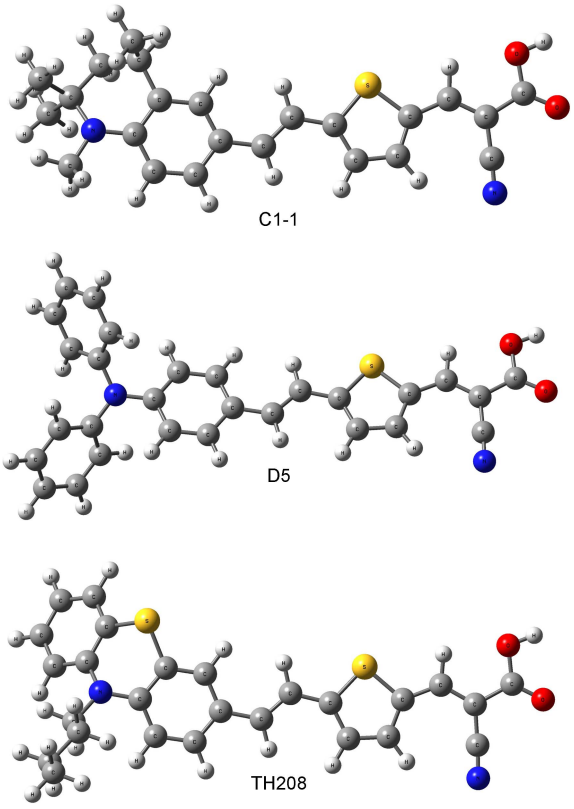

Figure 2. Optimized ground-state geometries of C1-1, D5 and TH208 computed at the B3LYP/6-31G(d) level.

anchoring carboxyl group (–COOH) is coplanar with the π extended system of the molecule, as demonstrated by the negligible C_7-C_8-C_{11}-O_{13} values. Therefore, assuming a bi-dentate bind of the carboxyl group to the supporting semiconductor's surface it can be inferred that the π system of these dyes most probably lay perpendicular to the surface, thus resulting in a dense package and coverage.[41] On the other hand, loss of planarity within the donor fragment can help to inhibit the close intermolecular π-π aggregation effectively.

Charge Analysis. To characterize the direction and magnitude of the charge transfer (CT) interaction between different parts of the molecule (particularly the acceptor and donor moieties), the SOPT analysis of the Fock matrix within the NBO basis was performed. In this procedure, the role of electronic delocalization can be evaluated quantitatively. The directly estimated approach of π-conjugative stable energies using the SOPT analysis will be very helpful to analyze the π-conjugation strength of the D-π-A dyes. The π-conjugation stabilization strength was evaluated by the NBO donor-acceptor interaction energies which are calculated on the basis of Lewis- and Pauling-like localized structural and hybridization theories and are presented with the classical π-conjugation concepts by a refinement of NBO analysis. This interaction energy corresponds to the charge delocalization due to the loss of electronic occupation from the localized Lewis molecular orbital to the non-Lewis molecular orbital leading to the distribution of electronic charge and therefore the perturbation from idealized Lewis structure description. For a characteristic conjugated π-bond network with two pairs of conjugated π bonds, the delocalized molecular orbitals can be pictured using the refined idealized Lewis structures by NBO donor-acceptor interaction of $\pi_a \rightarrow \pi_b^*$ and $\pi_a \rightarrow \pi_b^*$. According to the perturbation theory, the lowering energy due to $\pi_a \rightarrow \pi_b^*$ interaction, which is also referred to as the quantum mechanical resonance energy (denoted as QMRE), is estimated as[42]

$$\Delta E^{(2)}_{\psi\text{donor}\rightarrow\psi\text{acceptor}} \approx -2\cdot\frac{\mathrm{F(acc,\ don)}^2}{\mathrm{F}_{acc}-\mathrm{E}_{don}} \qquad (1)$$

where $E_{acc} - E_{don}$ is the energy difference of interacting NBO and the matrix element, and F(acc, don) is the off-diagonal element associated with the NBO Fock matrix. The strength of π-type conjugation and its variations by introducing resonance moieties can be conveniently visualized in terms of the NBO second order perturbation stabilization energies ($\Delta E^{(2)}_{\psi\text{donor}\rightarrow\psi\text{acceptor}}$) and the CT from π_a to π_b^*. The sum of stabilization energies is chosen as an indicator of the degree of the π-conjugation. According to the NBO donor-acceptor interaction theory, the charge occupancy of the π^* NBO also indicates the strength of π-conjugation. The quantities of transferred charge from a given donor to a given acceptor orbital may be estimated again using elementary perturbation theory arguments, leading to the following approximate formula:

$$q_{\text{donor}\rightarrow\text{acceptor}} \approx 2\left(\frac{\mathrm{F(acc,\ don)}}{\mathrm{F}_{acc}-\mathrm{E}_{don}}\right)^2 \qquad (2)$$

The selected NBO parameters from the SOPT analysis are presented in Table 1. The CT in these D-π-A dyes is remarkable and essentially one directional, from the donor to the acceptor. The NBO parameters from the donor to the acceptor for C1-1 are larger than those for D5 and TH208, pointing out that the electron-donating ability of the THQ unit is stronger than those of the TPA and PTZ groups.

Electronic Structures. In a simplified picture, the electronic transition during the light absorption process of dyes can be sketched as removal of an electron in the HOMO followed by electron addition to the LUMO. Thus, electron contribution of the frontier molecular orbitals (MOs) is very important in understanding the capabilities of an organic dye as photosensitizer in DSSCs.

Figure 3 shows the isodensity plots of the frontier MOs of C1-1, D5 and TH205. In all cases, the electron distributions between HOMO and LUMO are significantly different. The HOMO and HOMO-1 are delocalized over the entire molecule (including the donor); whereas the LUMO is delocalized essentially on the acceptor group with sizable contribution from the π-bridge. Thus, the HOMO-LUMO excitation on

Table 1. Conjugative interaction energies ($\Delta E^{(2)}$, in kcal/mol) and transferred charge (q, in e) between the π and π^* orbitals in C1-1, D5 and TH208 from the second-order perturbation theory analysis of the Fock matrix within the NBO analysis

Dye	Donor orbital	Acceptor orbital	$\Delta E^{(2)}$	E_{acc}-E_{don}/a.u.	F(acc, don)/a.u.	$q_{\text{donor}\rightarrow\text{acceptor}}$
C1-1	π(C1=C2)	π*(C3=C4)	29.01	0.51	0.115	0.102
	π(C3=C4)	π*(C1=C2)	2.07	1.81	0.055	0.002
	π(C7=C8)	π*(C9=C10)	43.83	0.53	0.138	0.136
	π(C9=C10)	π*(C7=C8)	11.52	0.52	0.073	0.039
D5	π(C1=C2)	π*(C3=C4)	22.16	0.51	0.102	0.080
	π(C3=C4)	π*(C1=C2)	13.45	0.53	0.081	0.047
	π(C7=C8)	π*(C9=C10)	42.13	0.54	0.136	0.127
	π(C9=C10)	π*(C7=C8)	11.67	0.53	0.073	0.038
TH208	π(C1=C2)	π*(C3=C4)	20.85	0.51	0.099	0.075
	π(C3=C4)	π*(C1=C2)	13.66	0.53	0.082	0.048
	π(C7=C8)	π*(C9=C10)	41.31	0.54	0.135	0.125
	π(C9=C10)	π*(C7=C8)	11.74	0.53	0.073	0.038

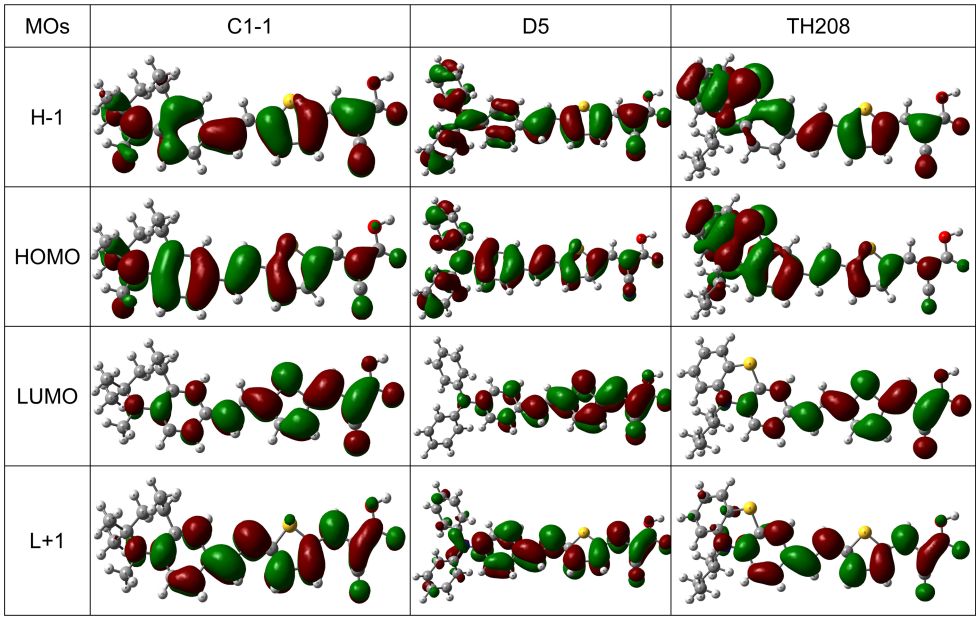

Figure 3. Isosurfaces of selected frontier orbitals of C1-1, D5 and TH208. The isovalue is 0.02 a.u.

these dyes induced by light irradiation could move the electron distribution from the donor moiety to the anchoring/acceptor moiety, consequently favoring electron injection from the dye to the semiconductor. At the same time, the electronic delocalization along the π-bridge ensures some overlap between the ground and excited states, which is important for achieving good molar extinction coefficients.

The calculated molecular orbital energy diagram for these D-π-A dyes is shown in Figure 4. In DSSC principle, the LUMO level of the dye must be situated above the semiconductor CB for effective electron injection, while the HOMO should be located under the redox couple of electrolyte for efficient regeneration of the oxidized dye. The edges of the valence band (VB) and CB of a TiO_2 anatase (101) surface are computed at −8.70 and −3.74 eV.[43] It can be found that for the dyes considered here, the simulated LUMO energies lie above the CB of TiO_2, providing the thermodynamic driving force for favorable interfacial electron injection from the excited dyes to the CB edge of TiO_2. Relatively large energy gaps between the LUMO energies of

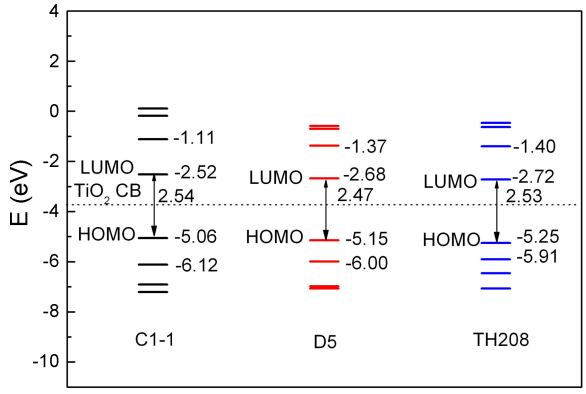

Figure 4. Frontier molecular orbital energies of C1-1, D5 and TH208.

these dyes and the semiconductor CB would be beneficial to the photovoltaic conversion efficiencies. On the other hand, the HOMOs of these dyes lie below the iodide redox potential (−4.8 eV[44]), giving rise to a fast dye regeneration and avoiding the geminate charge recombination between the oxidized dyes and the photo-injected electrons in the TiO_2 film. Both the HOMO and LUMO energies decrease when going from C1-1 to D5 (a decrease of 0.09 and 0.16 eV for HOMO and LUMO, respectively) and from D5 to TH208 (0.10 and 0.04 eV, respectively), further confirming the stronger electron-donating ability of THQ than TPA and PTZ (in agreement with the previously discussed charge results).

The open-circuit photovoltage V_{OC} in DSSCs can be determined by[45]:

$$V_{OC} = \frac{E_c}{q} + \frac{kT}{q}\ln\left(\frac{n_c}{N_{CB}}\right) - \frac{E_{redox}}{q} \quad (3)$$

where E_c is the CB edge of the semiconductor, E_{redox} is the electrolyte Fermi-level, kT is the thermal energy, q is the unit charge, n_c is the number of electrons in the CB, and N_{CB} is the accessible density of CB states. Upon the adsorption of dyes onto the semiconductor, the shift of E_c could be expressed as a function of the dipole moment of adsorbed dye as[46]:

$$\Delta CB = -\frac{q\mu_{normal}\gamma}{\varepsilon_0\varepsilon} \quad (4)$$

where q is the electron charge, ε_0 and ε are the permittivity of the vacuum and the dielectric constant of the organic monolayer, γ is the dye's surface concentration, and μ_{normal} is the component of dipole moment of the individual molecule perpendicular to the semiconductor surface. Grätzel and coworkers[47] have proven theoretically that the V_{OC} of DSSCs linearly increases with the μ_{normal} of the sensitizers pointing

outward from the semiconductor surface. The dipole moments of the free dyes were calculated by B3LYP/6-31G(d) at the geometry of dyes adsorbed onto TiO_2. The obtained normal dipole moments for C1-1, D5 and TH208 are 9.25, 9.70 and 9.70 Debye, respectively. The lower μ_{normal} of C1-1 would give rise to less negative charges located close to the semiconductor and thus result in a smaller CB energy level upshift as well as a smaller V_{OC}.[9]

Absorption Spectra. To gain insight into the intense absorption spectra of C1-1, D5 and TH208, TD-DFT calculations were performed based on the optimized ground-state geometries. The 30 lowest singlet-singlet transitions, up to an energy of 4.96 eV (250 nm), were taken into account. The excitation energies from TD-DFT calculations are generally within a 0.4 eV deviation from experimental data, and for organic dyes the average deviations are frequently smaller than this upper limit. For instance, Guillaumont and Nakamura[48] simulated the maximum absorption wavelength (λ_{max}) of several organic dyes (indigo, azobenzene, phenylamine, hydrazone, and anthraquinone) with an average error close to 0.20 eV. The establishment of an efficient computational framework highly depends on the appropriate choice of functionals and basis sets. Firstly, the vertical transitions from the S_0 state to the S_1 state were calculated in the frame of TD-DFT/LR-CPCM/6-31G(d) to evaluate the functional effects. Table 2 presents a comparison between the calculated λ_{max} using different functionals and the experimental λ_{max} for these dyes. The results indicate that the functionals have a remarkable effect on the vertical transition energies. The B3LYP functional underestimates the λ_{max} values very significantly (0.21, 0.45 and 0.36 eV for C1-1, D5 and TH208, respectively); MPW1B95 and PBE1PBE also deliver underestimated λ_{max} values. The other functionals with long-range corrections (CAM-B3LYP, LC-ωPBE and ωB97XD) overestimate the λ_{max} values. The λ_{max} and relative transition probabilities (intensities) from CAM-B3LYP agree best with the experimental data. Thus, CAM-B3LYP is the functional of choice for the absorption spectra calculation.

The selection of a basis set in the computation of electronically excited states is very important if one intends to obtain accurate results.[49] Usually, diffusion functions and polarization functions improve the calculated accuracy but at the increased computational cost. The compromise is to carry out computations using small basis sets and check for convergence using large basis sets. Therefore, we calculated the vertical transitions using CAM-B3LYP/6-31G(d), CAM-B3LYP/6-31+G(d, p) and CAM-B3LYP/6-311+G(2d,2p) based on the optimized ground-state geometries, respectively. The results for C1-1, D5 and TH208 using different basis sets are listed in Table 3. The deviations between the calculated and experimental data are reduced when additional polarization, diffuse, or valence functions are included. However, the computational time using 6-311+G(2d,2p) are much longer than using 6-31+G(d, p), accompanied with only negligible improvements in the results. Thus, 6-31+G(d, p) is the best compromise between computational cost and accuracy for the TD-DFT calculations of the as-investigated dyes.

The vertical excitation energies and oscillator strengths along with the main excitation configurations of the studied dyes calculated at the CAM-B3LYP/6-31+G(d, p) level are listed in Table 4. The corresponding simulated absorption spectra are depicted in Figure 5. The first optically allowed transition from $S_0 \rightarrow S_1$ for C1-1, D5 and TH208 are simulated to populate at 501, 477 and 461 nm, respectively. For this transition, the absolute deviation with respect to the experimental values of these dyes (525, 490 and 494 nm[9]) is below 35 nm, in agreement with the accuracy level expected at this level of theory.[49] The relative absorption intensities for C1-1, D5 and TH208 also agree well with those of the

Table 2. Functional effect on maximum absorption wavelength (λ_{max}, nm/eV) and absorption coefficient (ε, M^{-1} cm^{-1}) the studied dyes at 6-31G(d) level

	C1-1		D5		TH208	
	λ_{max}	ε	λ_{max}	ε	λ_{max}	ε
Expt.[9]	525/2.36	22000	490/2.53	29000	494/2.51	27000
B3LYP	576/2.15	102000	595/2.08	92000	578/2.15	67000
CAM-B3LYP	482/2.57	109000	465/2.67	139000	448/2.77	129000
LC-ωPBE	428/2.90	126000	414/3.00	143000	404/3.07	133000
ωB97XD	463/2.68	125000	450/2.76	144000	436/2.84	133000
MPW1B95	537/2.31	113000	539/2.30	111000	518/2.39	92000
PBE1PBE	555/2.23	108000	564/2.20	102000	544/2.28	79000

Table 3. Basis set effect on λ_{max} (nm/eV) and *f* (a.u.) for the studied dyes using CAM-B3LYP

	C1-1		D5		TH208	
	λ_{max}	*f*	λ_{max}	*f*	λ_{max}	*f*
6-31G(d)	482/2.57	1.5176	465/2.67	1.9221	448/2.77	1.7812
6-31+G(d,p)	501/2.47	1.5075	477/2.60	1.9256	461/2.69	1.7838
6-311+G(2d,2p)	504/2.46	1.5208	479/2.59	1.9416	463/2.68	1.7909

Table 4. Selected excitation energies (eV/nm), electronic transition configurations, oscillator strengths (a.u.) and LHE for C1-1, D5 and TH208 in CH_2Cl_2 at CAM-B3LYP/6-31+G(d,p) level (H=HOMO, L=LUMO, L+1=LUMO+1, etc.)

Dye	State	Configuration	λ_{max}	f	LHE
C1-1	$S_0 \rightarrow S_1$	H → L (+86%); H-1 → L (−7%)	501.2/2.47	1.5075	0.9689
	$S_0 \rightarrow S_2$	H-1 → L (+77%); H → L+1 (+6%)	322.7/3.84	0.1625	
D5	$S_0 \rightarrow S_1$	H → L (+78%); H-1 → L (+15%)	477.4/2.60	1.9256	0.9881
	$S_0 \rightarrow S_3$	H → L+1 (+46%); H-1 → L (+15%); H → L+2 (+14%); H → L (−10%)	307.1/4.04	0.1222	
	$S_0 \rightarrow S_5$	H → L+3 (+81%); H-1 → L+3 (−13%)	283.9/4.37	0.2619	
TH208	$S_0 \rightarrow S_1$	H → L (+75%); H-1 → L (−17%)	460.9/2.69	1.7838	0.9835

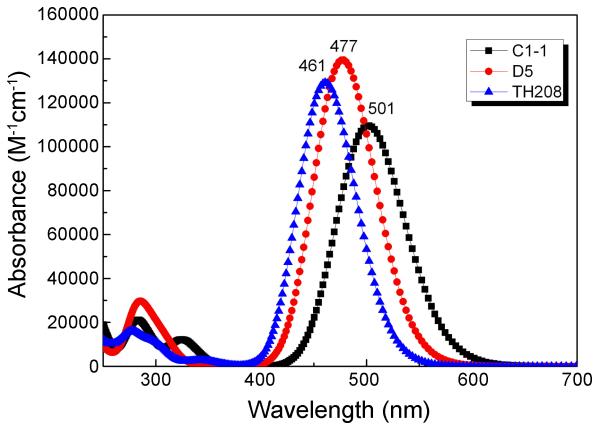

Figure 5. Simulated absorption spectra of C1-1, D5 and TH208 in CH_2Cl_2 at the CAM-B3LYP/6-31+G(d,p) level.

experiment (C1-1: 22000 M^{-1} cm^{-1}, D5: 29000 M^{-1} cm^{-1} and TH208: 27000 M^{-1} cm^{-1} [9]). However, the close λ_{max} values between D5 and TH208 are not correctly reproduced. This band for these dyes corresponds to the HOMO → LUMO and HOMO-1 → LUMO transitions, and is of charge transfer character thus possessing high transition intensity.

The spectral response of DSSCs is determined by the monochromatic incident photon-to-current conversion efficiency (IPCE), which can be expressed as follows[7]:

$$IPCE(\lambda) = LHE(\lambda)\varphi_{inj}(\lambda)\varphi_{reg}\eta_{coll}(\lambda) \quad (5)$$

where LHE(λ) is the light-harvesting efficiency (LHE(λ) = 1 − 10^{-f}), φ_{inj} and φ_{reg} are the quantum yields for electron injection and dye regeneration, and η_{coll} is the electron collection efficiency. The relatively lower IPCE of the DSSC based on C1-1[9] can be attributed to the smaller oscillator strength of C1-1, leading to the relatively smaller LHE.

Conclusions

In this paper, the geometrical and electric structures of three D-π-A-type organic dyes (C1-1, D5 and TH208) with different electron-donating groups (THQ, TPA and PTZ) used for DSSC were investigated by DFT calculations. The UV-vis absorption spectra were simulated by TD-DFT calculations. The calculated geometries indicate that the strong conjugation is formed in these dyes. The NBO results suggest that there are some charges transferred from the donor to the acceptor, and the electron-donating ability of the THQ unit is stronger than those of the TPA and PTZ groups. The electron distributions and energy levels of frontier molecular orbitals of these dyes are beneficial to the charge separation between the donor and acceptor as well as the electron injection from the excited dye into the semiconductor CB. The CAM-B3LYP/6-31+G(d, p) provides acceptable simulated absorption spectra, with absolute deviation to the experimental values below 0.18 eV. The first optically allowed transition from $S_0 \rightarrow S_1$ for these dyes is attributed to the HOMO → LUMO and HOMO-1 → LUMO transitions. The relatively low V_{OC} and IPCE of the DSSC based on C1-1 are ascribed to the small normal dipole moment and oscillator strength of this dye, respectively.

Acknowledgments. This work was supported by the Natural Science Foundation of China (No. 51003082 and No. 61108033), the Natural Science Foundation of Hubei Province (No. 2012FFB046) and the Young People Project of Wuhan Science and Technology Bureau (No. 201271031381). The authors gratefully wish to express their thanks to the reviewers for critically reviewing the manuscript and making important suggestions. And the publication cost of this paper was supported by the Korean Chemical Society.

References

1. O'Regan, B.; Grätzel, M. *Nature* **1991**, *353*, 737.
2. Nazeeruddin, M. K.; Angelis, F. D.; Fantacci, S.; Selloni, A.; Viscardi, G.; Liska, P.; Ito, S.; Takeru, B.; Grätzel, M. *J. Am. Chem. Soc.* **2005**, *127*, 16835.
3. Gao, F.; Wang, Y.; Shi, D.; Zhang, J.; Wang, M.; Jing, X.; Humphry-Baker, R.; Wang, P.; Zakeeruddin, S. M.; Grätzel, M. *J. Am. Chem. Soc.* **2008**, *130*, 10720.
4. Chen, C.-Y.; Wang, M.; Li, J.-Y.; Pootrakulchote, N.; Alibabaei, L.; Ngoc-le, C.-H.; Decoppet, J.-D.; Tsai, J.-H.; Grätzel, C.; Wu, C.-G.; Zakeeruddin, S. M.; Grätzel, M. *ACS Nano* **2009**, *3*, 3103.
5. Amao, Y.; Komori, T. *Biosensors Bioelectron.* **2004**, *19*, 843.
6. Mishra, A.; Fischer, M. K. R.; Bäuerle, P. *Angew. Chem. Int. Ed.* **2009**, *48*, 2474.
7. Hagfeldt, A.; Boschloo, G.; Sun, L.; Kloo, L.; Pettersson, H. *Chem. Rev.* **2010**, *110*, 6595.
8. Nazeeruddin, M. K.; Péchy, P.; Renouard, T.; Zakeeruddin, S. M.; Humphry-Baker, R.; Comte, P.; Liska, P.; Cevey, L.; Costa, E.; Shklover, V.; Spiccia, L.; Deacon, G. B.; Bignozzi, C. A.; Grätzel, M. *J. Am. Chem. Soc.* **2001**, *123*, 1613.
9. Tian, H.; Yang, X.; Cong, J.; Chen, R.; Teng, C.; Liu, J.; Hao, Y.;

Wang, L.; Sun, L. *Dyes Pigm* **2010**, *84*, 62.
10. Xu, J.; Wang, L.; Liang, G.; Bai, Z.; Wang, L.; Xu, W.; Shen, X. *Bull. Korean Chem. Soc.* **2010**, *9*, 2531.
11. Barolo, C.; Nazeeruddin, M. K.; Fantacci, S.; Di Censo, D.; Comte, P.; Liska, P.; Viscardi, G.; Quagliotto, P.; De Angelis, F.; Ito, S.; Gratzel, M. *Inorg. Chem.* **2006**, *45*, 4642.
12. Onozawa-Komatsuzaki, N.; Kitao, O.; Yanagida, M.; Himeda, Y.; Sugihara, H.; Kasuga, K. *New J. Chem.* **2006**, *30*, 689.
13. Fantacci, S.; De Angelis, F.; Selloni, A. *J. Am. Chem. Soc.* **2003**, *125*, 4381.
14. Kurashige, Y.; Nakajima, T.; Kurashige, S.; Hirao, K.; Nishikitani, Y. *J. Phys. Chem. A* **2007**, *111*, 5544.
15. Zhang, X.; Zhang, J.-J.; Xia, Y.-Y. *J. Photochem. Photobiol. A: Chem.* **2008**, *194*, 167.
16. Liu, Z. *J. Mol. Struct. (Theochem)* **2008**, *862*, 44.
17. Ma, R.; Guo, P.; Cui, H.; Zhang, X.; Nazeeruddin, M. K.; Grätzel, M. *J. Phys. Chem. A* **2009**, *113*, 10119.
18. Kumar, P. S.; Vasudevan, K.; Prakasam, A.; Geetha, M.; Anbarasan, P. M. *Spectrochim. Acta A: Mol. Biomol. Spectrosc.* **2010**, *77*, 45.
19. Xu, J.; Wang, L.; Liang, G.; Bai, Z.; Wang, L.; Xu, W.; Shen, X. *Spectrochim. Acta A: Mol. Biomol. Spectrosc.* **2011**, *78*, 287.
20. Senthilkumar, P.; Anbarasan, P. M. *J. Mol. Model* **2011**, *17*, 49.
21. Xu, J.; Zhu, L.; Fang, D.; Chen, B.; Liu, L.; Wang, L.; Xu, W. *ChemPhysChem.* **2012**, *13*, 3320.
22. Xu, J.; Zhang, H.; Wang, L.; Liang, G.; Wang, L.; Shen, X.; Xu, W. *Monatsh. Chem.* **2010**, *141*, 549.
23. Xu, J.; Liang, G.; Wang, L.; Xu, W.; Cui, W.; Zhang, H.; Li, Z. *J. Serb. Chem. Soc.* **2010**, *75*, 259.
24. Wang, X.; Xu, J.; Li, M.; Fang, D.; Chen, B.; Wang, L.; Xu, W. *RSC Adv.* **2013**, *3*, 5227.
25. Xu, J.; Wang, L.; Liu, L.; Bai, Z.; Wang, L.; Liang, G.; Shen, X.; Xu, W. *Can. J. Chem.* **2011**, *89*, 978.
26. Zhang, C.-R.; Liu, Z.-J.; Chen, Y.-H.; Chen, H.-S.; Wu, Y.-Z.; Yuan, L.-H. *J. Mol. Struct. (THEOCHEM)* **2009**, *899*, 86.
27. Song, J. *J. Chem. Soc. Pak.* **2012**, *34*, 1416.
28. Frisch, M. J.; Trucks, G. W.; Schlegel, H. B.; Scuseria, G. E.; Robb, M. A.; Cheeseman, J. R.; Scalmani, G.; Barone, V.; Mennucci, B.; Petersson, G. A.; Nakatsuji, H.; Caricato, M.; Li, X.; Hratchian, H. P.; Izmaylov, A. F.; Bloino, J.; Zheng, G.; Sonnenberg, J. L.; Hada, M.; Ehara, M.; Toyota, K.; Fukuda, R.; Hasegawa, J.; Ishida, M.; Nakajima, T.; Honda, Y.; Kitao, O.; Nakai, H.; Vreven, T.; Montgomery, J. A.; Peralta, J. J. E.; Ogliaro, F.; Bearpark, M.; Heyd, J. J.; Brothers, E.; Kudin, K. N.; Staroverov, V. N.; Kobayashi, R.; Normand, J.; Raghavachari, K.; Rendell, A.; Burant, J. C.; Iyengar, S. S.; Tomasi, J.; Cossi, M.; Rega, N.; Millam, J. M.; Klene, M.; Knox, J. E.; Cross, J. B.; Bakken, V.; Adamo, C.; Jaramillo, J.; Gomperts, R.; Stratmann, R. E.; Yazyev, O.; Austin, A. J.; Cammi, R.; Pomelli, C.; Ochterski, J. W.; Martin, R. L.; Morokuma, K.; Zakrzewski, V. G.; Voth, G. A.; Salvador, P.; Dannenberg, J. J.; Dapprich, S.; Daniels, A. D.; Farkas, O.; Foresman, J. B.; Ortiz, J. V.; Cioslowski, J.; Fox, D. J., Gaussian Inc.: Wallingford CT, 2009.
29. Becke, A. D. *J. Chem. Phys.* **1993**, *98*, 5648.
30. Lee, C.; Yang, W.; Parr, R. G. *Phys. Rev. B* **1988**, *37*, 785.
31. Møller, C.; Plesset, M. S. *Phys. Rev.* **1934**, *46*, 618.
32. Yanai, T.; Tew, D.; Handy, N. *Chem. Phys. Lett.* **2004**, *393*, 51.
33. Vydrov, O. A.; Scuseria, G. E. *J. Chem. Phys.* **2006**, *125*, 234109.
34. Vydrov, O. A.; Heyd, J.; Krukau, A.; Scuseria, G. E. *J. Chem. Phys.* **2006**, *125*, 074106.
35. Chai, J.-D.; Head-Gordon, M. *Phys. Chem. Chem. Phys.* **2008**, *10*, 6615.
36. Zhao, Y.; Truhlar, D. G. *J. Phys. Chem. A* **2004**, *108*, 6908.
37. Adamo, C.; Barone, V. *J. Chem. Phys.* **1999**, *110*, 6158.
38. Cossi, M.; Barone, V.; Cammi, R.; Tomasi, J. *Chem. Phys. Lett.* **1996**, *255*, 327.
39. Barone, V.; Cossi, M. *J. Phys. Chem. A* **1998**, *102*, 1995.
40. Gorelsky, S. I. University of Ottawa: Ottawa, Canada, 2010.
41. Howie, W. H.; Claeyssens, F.; Miura, H.; Peter, L. M. *J. Am. Chem. Soc.* **2008**, *130*, 1367.
42. King, B. F.; Weinhold, F. *J. Chem. Phys.* **1995**, *103*, 333.
43. Bahers, T. L.; Pauporté, T.; Scalmani, G.; Adamo, C.; Ciofini, I. *Phys. Chem. Chem. Phys.* **2009**, *11*, 11276.
44. Cahen, D.; Hodes, G.; Grätzel, M.; Guillemoles, J. F.; Riess, I. *J. Phys. Chem. B* **2000**, *104*, 2053.
45. Marinado, T.; Nonomura, K.; Nissfolk, J.; Karlsson, M. K.; Hagberg, D. P.; Sun, L.; Mori, S.; Hagfeldt, A. *Langmuir* **2010**, *26*, 2592.
46. Rühle, S.; Greenshtein, M.; Chen, S.-G.; Merson, A.; Pizem, H.; Sukenik, C. S.; Cahen, D.; Zaban, A. *J. Phys. Chem. B* **2005**, *109*, 18907.
47. Chen, P.; Yum, J.-H.; Angelis, F. D.; Mosconi, E.; Fantacci, S.; Moon, S.-J.; Baker, R. H.; Ko, J.; Nazeeruddin, M. K.; Gratzel, M. *Nano. Lett.* **2009**, *9*, 2487.
48. Guillaumont, D.; Nakamura, S. *Dyes Pigm.* **2000**, *46*, 85.
49. Jacquemin, D.; Perpète, E. A.; Ciofini, I.; Adamo, C. *Acc. Chem. Res.* **2009**, *42*, 326.